JAAS

ROYAL SOCIETY OF CHEMISTRY

PAPER

View Article Online
View Journal | View Issue

Cite this: *J. Anal. At. Spectrom.*, 2025, **40**, 2803

Introducing MC-MICAP-MS: using a N_2-based plasma ion source for Sr isotope abundance ratio measurements

Anika Retzmann, *[a] Ashok Menon[b] and Michael E. Wieser [a]

High-precision metal(loid) isotope abundance ratios are a powerful research tool across various disciplines. These ratios are typically measured using multi-collector mass spectrometry with ion sources such as gas source, thermal ionization, or inductively coupled plasma (*i.e.*, IRMS, TIMS, and MC-ICP-MS). This study presents the first integration of the recently developed microwave inductively coupled atmospheric-pressure plasma (MICAP) ion source, which sustains a plasma using N_2, with a multi-collector mass spectrometer and offers the first characterization of the resulting MC-MICAP-MS instrument for high-precision metal isotope abundance ratio measurements. The performance of the MC-MICAP-MS instrument was evaluated by measuring Sr isotope abundance ratios and directly comparing the results with those obtained using established technology (*i.e.*, MC-ICP-MS) with an Ar-ICP as the ion source. Initial results using the MICAP ion source show that the $^{87}Sr/^{86}Sr$ intensity ratio precision (approx. 0.007%) and the repeatability of the $^{87}Sr/^{86}Sr$ intensity ratio (approx. 0.010%), as well as the intermediate precision of the conventional $^{87}Sr/^{86}Sr$ isotope abundance ratio (approx. 0.0013%) are fully comparable to those of conventional MC-ICP-MS systems. The instrumental isotopic fractionation (IIF) observed for the new MC-MICAP-MS instrument was predominantly mass-dependent for Sr. This allowed the successful application of common IIF correction strategies, such as internal normalisation and standard-sample bracketing, for the determination of Sr isotope abundance ratios. The conventional $^{87}Sr/^{86}Sr$ isotope abundance ratios and $\delta^{88}Sr/^{86}Sr_{SRM987}$ values measured for various geological and biological reference materials (*i.e.*, seawater, basalt, slate, and bone) using MC-MICAP-MS were consistent with previously reported values obtained from established technologies such as TIMS and MC-ICP-MS. Overall, this study demonstrates that MICAP is an applicable and viable alternative ion source for multi-collector mass spectrometry, maintaining both double-focusing properties and high-precision performance without compromising the accuracy and reliability of the measurement results.

Received 11th July 2025
Accepted 19th August 2025

DOI: 10.1039/d5ja00271k

rsc.li/jaas

1. Introduction

Over the last few decades, the high-precision analysis of radiogenic and stable isotope abundance ratios of various metal(loid)s has evolved into a powerful research tool with applications in diverse fields,[1] such as geosciences, environmental sciences,[2] archaeological sciences,[3,4] nuclear and forensic sciences,[5] ecological and food sciences,[6,7] and biomedical sciences.[8,9] The variations in radiogenic and stable metal(loid) isotopic compositions are significant and measurable when using appropriate methods and suitable calibration strategies. Since the early years of mass spectrometry, gas source isotope ratio mass spectrometry (IRMS) has been the leading technique to measure isotopic variability of light elements (H, C, O, N, and S). Thermal ionization has been used as an additional ion source for high-precision mass spectrometry (*i.e.*, TIMS) to measure the isotopic composition of various metals and metalloids, since the second half of the 20th century.[6] In 1992, the first multi-collector detector array was coupled to an inductively coupled plasma (ICP) as the ion source for high-precision isotope mass spectrometry (*i.e.*, MC-ICP-MS).[10] Over the last few decades, MC-ICP-MS has developed into a well-established technique for isotope abundance ratio measurements that provides straightforward sample introduction, rapid analysis at high-precision, and the capability to analyze almost the entire periodic table of the elements.[6] Today, these three mass spectrometric techniques (*i.e.*, IRMS, TIMS, and MC-ICP-MS) can be regarded as key techniques in the field of radiogenic and stable metal(loid) isotope abundance ratio analysis.[6] They are all magnetic sector field mass spectrometers, and their high-precision performance can be attributed mainly to two features: multiple collectors and wide, flat-topped peaks. A magnetic field is used to separate ions along a focal plane based on their mass-to-charge (m/z) ratio and an array of several parallel detectors is arranged to

[a]*University of Calgary, Department of Physics and Astronomy, 2500 University Dr NW, Calgary, AB T2N 1N4, Canada. E-mail: anika.retzmann@ucalgary.ca*
[b]*Radom Instruments LLC, N27W23676 Paul Rd, Pewaukee, WI 53072, USA*

collect the ions of the isotopes of interest simultaneously. In this configuration, any changes in the ion source conditions affect all ions in a similar manner and therefore have only minimal effect on the determination of isotope abundance ratios, thus providing the opportunity for high-precision measurement of isotopic composition.[11] The flat-topped peaks have an important advantage that small variations in the position of the peak in the focal plane of the detectors (*i.e.*, mass shifts), caused by small variations in electric or magnetic fields, do not significantly affect the determination of isotope abundance ratios, again providing high-precision.[11,12]

Metrologically sound measurement protocols for the determination of high-precision metal(loid) isotope abundance ratios by multi-collector mass spectrometry must consider the contribution and correction of interferences and instrumental isotopic fractionation (IIF, aka mass bias, mass discrimination).[6] Metal(loid) isotope abundance ratio analysis can suffer from spectral and non-spectral interferences: Spectral interferences are additional signals detected at the same m/z ratio as the analyte ions that originate from elemental isobaric ions (*e.g.*, $^{87}Rb^+$ on $^{87}Sr^+$ and $^{40}Ar^+$ on $^{40}Ca^+$), doubly charged ions (*e.g.*, REE^{++} on Sr isotopes and $^{40}Ar^{4+}$ on $^{10}B^+$), and polyatomic ions (*e.g.*, $CaCa^+$ on Sr isotopes and $^{40}Ar^{16}O^+$ on $^{56}Fe^+$). The non-spectral interferences refer mainly to matrix effects (*e.g.*, Na, Mg, K, Ca, and Fe) and lead to suppression or enhancement of signals, signal instability and changes in the IIF behaviour.[12,13] IIF includes all instrumental discrimination effects that occur during sample introduction, ion formation, ion extraction, ion transmission, ion separation and ion detection in the mass spectrometer, and that may result in significantly biased isotope abundance ratios with respect to the true value.[1,14] The understanding of the underlying physics and factors that cause IIF phenomena in plasma-based mass spectrometry is still very limited,[6,15,16] but supersonic expansion and space charge effects account for most of the resulting IIF in plasma-based mass spectrometry; both processes favor the transmission of heavier isotopes.[14,15] These sources of IIF are mass-dependent in nature. However, recent studies have shown variations in isotopic fractionation for different isotope pairs of the same element within the MC-ICP-MS itself. This type of IIF does not follow the empirical mass-dependent fractionation law and has been termed mass-independent fractionation. The exact causes of this phenomenon are still under debate.[1,15] The nature of IIF, its behaviour and stability throughout the measurement, have significant impacts on the choice of the IIF correction model to determine reliable and precise isotope abundance ratios.[1] Common IIF correction models are discussed in detail elsewhere.[1,14,17,18]

The ion sources (*i.e.*, gas source, thermal ionization, and Ar-ICP) currently used for multi-collector mass spectrometry have limitations and pose different analytical challenges for high-precision isotope abundance ratio measurements. For example, ICP introduces relatively large IIF, that may include mass-independent behaviour, and Ar-based interferences that cannot be or can only partially be resolved.[1] Instrumental strategies to cope with the latter include, on the one hand, large geometry instruments that provide extra-high mass resolution to resolve polyatomic interferences[19,20] and, on the other hand, instruments that are equipped with a collision/reaction cell between the ion source and the ion separation stage to enable chemical resolution of isobaric interferences.[21–23] However, an alternative strategy could be the use of a different plasma ion source. Investigations into microwave-induced plasma (MIP) as an alternative ion source to Ar-ICP for elemental mass spectrometry date back to the 1960s.[24] The earlier designs of MIP were limited by low plasma power ($\leq$500 W) which resulted in inefficient atomization of the analytes from introduced solutions, and often required the introduction of a dried sample aerosol.[25–27] More recently, high-power MIPs were introduced that exhibited performance comparable to Ar-ICP, and were later commercialized as an alternatives to Ar-ICP-OES.[28–31] In a recent study, Lin *et al.* presented the first successful integration of a low-pressure He-MIP with a multi-collector mass spectrometer (*i.e.*, based on a Neptune MC-ICP-MS) to overcome the limitations of the ICP for isotope abundance ratio measurements.[32] They demonstrated the ability of the new instrument to deliver reliable and precise isotope abundance data (*i.e.*, $^{18}O/^{16}O$), owing to the generation of flat-topped peaks and the use of simultaneous ion detection. In this present study, the possibility of replacing the ICP ion source of a MC-ICP-MS instrument with the recently developed microwave inductively coupled atmospheric-pressure plasma (MICAP) as an alternative ion source is explored. This new instrument is termed MC-MICAP-MS. The MICAP is the newest design of microwave-induced plasma (MIP) ion sources, and enables a plasma to be sustained with N_2.[24] Both the radiofrequency ICP using Ar as the plasma gas and the MICAP using N_2 as the plasma gas are atmospheric-pressure inductively coupled plasma ion sources, although the means of generating the inductive field that transfers power to the plasma are different. The MICAP ion source uses a dielectric resonator ring (technical ceramic) that forms a high-frequency polarization current when exposed to a microwave field from the cavity magnetron. The polarization current, in turn, generates an orthogonal magnetic field that can support an annular plasma in N_2, obviating the need for Ar.[33] The plasma generated from the MICAP has improved homogeneity and can atomize, excite, and ionize the samples from gaseous, liquid, and even laser ablation (solid particle) sample introduction,[24,33,34] similar to Ar-ICP. Designed and marketed by Radom Instruments LLC, the MICAP ion source has been combined with single collector mass spectrometry,[33,34] replacing the Ar-ICP as the ion source for elemental analysis. From the comparison of Ar-ICP-MS and N_2-MICAP-MS it has been seen that the degree of ionization is comparable for Ar- and N_2-plasmas, and consequently only minor compromises are observed for several elements.[29] The analyte sensitivity is slightly lower for MICAP-MS as compared to ICP-MS for most elements, but the differences are less than an order of magnitude.[33] The N_2-MICAP ion source is comparable to the Ar-ICP ion source in terms of robustness and strong matrix tolerance.[24,33,35,36] Finally, the background signal of the N_2-MICAP contains significantly fewer interferences originating from plasma species than Ar-ICP.[34] Looking at the background spectrum, all major Ar-derived species, such as Ar^+, ArH^+, ArC^+,

ArN^+, ArO^+, and Ar_2^+ are absent, and many low-mass oxygen species (O^+, OH^+, and H_2O^+) are less intense compared to those observed with the Ar-ICP.[33,34] Most plasma species in MICAP have a m/z ratio below 35, which corresponds to N-related species,[36] and so a larger background-free region is available than in Ar-ICP-MS.[28] The most abundant background species are NO^+, N_2^+, N^+, N_3^+, O_2^+, N_4^+, O^+, and H_2O^+, and N_2-MICAP is found to be prone to oxide formation.[33,34] However, to the authors' knowledge, this revolutionary device has not yet been reported in combination with a high-precision multi-collector mass spectrometer such as the Thermo Fisher Scientific Neptune MC-ICP-MS to enable high-precision metal(loid) isotope abundance analysis.

The goal of the present study is to demonstrate the applicability of the MICAP as an ion source for multi-collector mass spectrometry and to evaluate the performance of the new MC-MICAP-MS instrument for high-precision metal isotope abundance ratio measurements. For this purpose, the isotopic system of Sr was investigated, which is neither influenced by Ar-based interferences nor by N-based interferences[33] and, furthermore, it is a well-characterized isotopic system. This enables a direct comparison of the performance between the new MC-MICAP-MS instrument and the established technology, *i.e.*, MC-ICP-MS. In addition, Sr has four stable isotopes which allows an investigation of the nature of IIF of the new MC-MICAP-MS instrument.

2. Experimental section

The MICAP ion source was combined with a multi-collector mass spectrometer in the Department of Physics and Astronomy at University of Calgary, Canada.

2.1. Instrumentation: MC-MICAP-MS

The MICAP ion source for mass spectrometry was purchased from Radom Instruments LLC (Pewaukee, WI, USA). In brief, the MICAP consists of a cavity magnetron that generates a microwave field (1500 W), an aluminum waveguide to direct the microwaves to the resonator chamber, an inductive iris for impedance matching, a dielectric resonator ring that is placed concentrically with a torch, a torch assembly to hold the torch, and an aluminum ring to tune the dielectric ring's resonance frequency.[24,33] Mounted vertically within the assembly is a conventional quartz ICP torch with a 1.5 mm injector (Glass Expansion Inc, Pocasset, MA, USA).

The unique symbiotic design of the MC-MICAP-MS instrument was constructed using a double-focusing Neptune MC-ICP-MS platform (Thermo Fisher Scientific, Bremen, Germany), equipped with a magnetic mass analyzer and a multiple ion detector platform (*i.e.*, nine Faraday cups (eight movable) and a dispersion of 17%), and the MICAP (Radom Instruments LLC) as the ion source (see Fig. 1A). The original ICP module of the Neptune was moved aside by fully opening the bench, and the MICAP ion source was installed at the vacuum interface next to the sampler cone. The MICAP ion source was mounted onto an *XYZ* stage which was positioned on a baseplate fixed to the sliding-rod of the open Neptune bench (see Fig. 1B and C). In this position, the plasma exhaust of the Neptune was used for the MICAP ion source. The power for the cavity magnetron of the MICAP was supplied by the Neptune using the 230 VAC supply originally used for the Neptune's RF generator. The water cooling for the cavity magnetron of the MICAP was also supplied by the Neptune. The plasma bench interlock was modified to remain permanently closed, which is not a concern since the Ar plasma is not being used with the MICAP in position. No other hardware modifications to the Neptune were required and the Neptune could be operated normally, except for the control of the N_2-based plasma.

The plasma ignition of the MICAP is accomplished in a computer-controlled sequence of MICAP-MS software (Radom Instruments LLC). In brief, a N_2 cooling gas flow of 14 L min^{-1} is provided to the ICP torch while microwave power (1.5 kW) is applied to the waveguide and resonator. Simultaneously, a small volume of Ar (99.999% purity, Air Liquide, Calgary, Canada) with a flow of 1.5 L min^{-1} is introduced into the torch as an auxiliary gas and a Tesla coil generates a series of sparks within the gas line to facilitate plasma ignition. Once the plasma is ignited, the Ar flow is stopped and the plasma is sustained solely with N_2 cooling gas, N_2 auxiliary gas, and N_2 carrier gas, all supplied from a liquid N_2 Dewar (99.999% purity, Air Liquide, Calgary, Canada).

2.1.1 Performance check. The peak shape, sensitivity, and isotope abundance ratio precision of the new MC-MICAP-MS instrument were compared to the performance of the Neptune platform when using Ar-ICP as the ion source. For the peak shape, a peak scan was performed over the mass range from 85.802 u to 86.017 u with 50 steps. Sensitivity was calculated from the abundance of $^{88}Sr^+$, the Sr concentration in the NIST SRM 987 solution and the signal intensity of $^{88}Sr^+$ under wet and dry sample introduction conditions. Intensity ratio precision (aka internal precision) is expressed as the RSD and refers to the standard deviation of N runs averaged to one measurement result. The repeatability of the intensity ratios is expressed as RSD and refers to the standard deviation of N measurements taken within a day. The intermediate precision (aka long-term precision) of the conventional $^{87}Sr/^{86}Sr$ isotope abundance ratio is expressed as RSD and refers to the standard deviation of N measurements collected over several days.

2.1.2 Instrumental isotopic fractionation. A series of experiments were performed to investigate the IIF behaviour, its stability, and its nature for the new MC-MICAP-MS instrument. The IIF per mass unit for B, Sr, and Pb was calculated in accordance with standard protocols.[15,37,38] The long-term stability of IIF was evaluated based on the RSD of 20–21 measurements of NIST SRM 987 solution over a measurement sequence of 5–9 hours. The effect of plasma conditions (*i.e.*, radial and axial position, nebulizer gas flow, and microwave plasma power) on the magnitude of IIF was investigated for the new MC-MICAP-MS instrument. Finally, the nature of the IIF was assessed using a three-isotope plot for Sr and the applicability of common IIF strategies (*i.e.*, internal normalization and standard-sample bracketing) was tested as well.

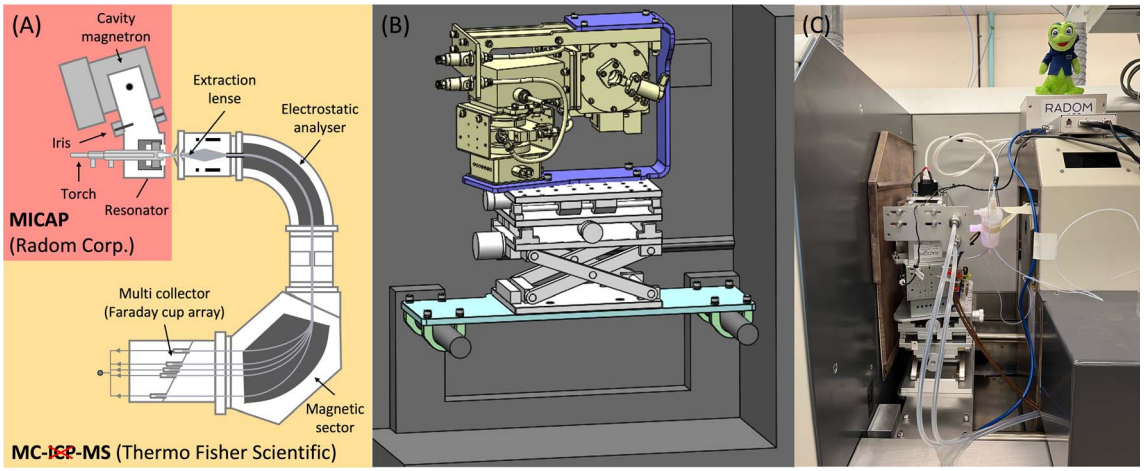

Fig. 1 (A) Schematic of MC-MICAP-MS, (B) CAD drawing of the design for mounting of the MICAP in the Neptune platform, and (C) MICAP installed in the Neptune platform.

2.1.3 Geological and biological reference materials. The accuracy of Sr isotope abundance measurements with the new MC-MICAP-MS instrument was investigated by using three geological reference materials (*i.e.*, seawater, basalt, and slate) and two biological reference materials (*i.e.*, bone ash and bone meal) after sample digestion and Sr purification. The determined conventional $^{87}Sr/^{86}Sr$ isotope abundance ratios and $\delta^{88}Sr/^{86}Sr_{SRM987}$ values of these materials were then compared to previously reported Sr isotopic compositions obtained using TIMS and MC-ICP-MS instruments.

2.2. Materials, reagents & reference materials

High-quality water (HQ water, Type I reagent-grade water (18.2 MΩ cm)) was obtained from a purification system (PURELAB Plus, U.S. FILTER, ELGA LabWater, High Wycombe, UK). Analytical reagent-grade nitric acid ($w(HNO_3)$ = 67–70%, Aristar Plus, VWR International, Radnor, PA, USA) and analytical reagent-grade hydrochloric acid ($w(HCl)$ = 34–37%, Aristar Plus, VWR International) were purified by double-subboiling using an acid purification system (Savillex, Eden Prairie, MN, USA). Hydrogen peroxide ($w(H_2O_2)$ = 30%, Fisher Scientific, Ottawa, Canada) and hydrofluoric acid (Environmental Grade Plus, Anachemia, VWR International) were used for sample digestion without any further purification. Diluted boric acid ($w(B(OH)_3)$ = 2%) was prepared from NIST SRM 951 (National Institute of Standards and Technology (NIST), Gaithersburg, MD, USA) in 5 mol L^{-1} hydrochloric acid. Before use, centrifuge tubes (1.5 mL, VWR International), DigiTUBE (50 mL, SCP Science, Quebec, Canada) and pipette tips (Eppendorf, Mississauga, Canada; Corning Incorporated, Corning, NY, USA; Fisherbrand, Fisher Scientific, USA) were leached for at least one week with dilute nitric acid ($w(HNO_3)$ ≈ 3%). Perfluoroalkoxy (PFA) screw cap vials (Savillex) were pre-cleaned using a two-step acid cleaning procedure with double-subboiled nitric acid.

The Sr resin (Eichrom Technologies, Lisle, IL, USA) was soaked in HQ water before use. One-milliliter empty cartridges and frits (AC-100-R01, TrisKem International, Bruz, France) were pre-cleaned and stored in diluted nitric acid ($w(HNO_3)$ ≈ 10%).

The following reference materials were analyzed in this study: IAPSO (Standard Seawater, Ocean Scientific International Ltd, Hampshire, UK), BCR-2 (Columbia River Basalt, United States Geological Survey, Denver, CO, USA), OU6 (Penrhyn Slate, International Association of Geoanalysts, Nottingham, UK), NIST SRM 1400 (bone ash, NIST), and NIST SRM 1486 (bone meal, NIST). NIST SRM 987 (NIST), which is certified for absolute Sr isotopic composition, was used as a quality control (QC) sample, as an isotope reference material for standard-sample bracketing during MC-MICAP-MS measurements and as δ-anchor for relative Sr isotopic analyses as recommended.[39] NIST SRM 951 (NIST) and NIST SRM 981 (NIST), which are certified for absolute B and Pb isotopic compositions, respectively, were used for the calculation of IIF per mass unit.

2.3. Analytical procedure

All sample preparation procedures were accomplished in a class 1000 cleanroom under a HEPA filter (Design Filtration Microzone, Ottawa, ON, Canada) to minimize blank levels and risk of contamination.

2.3.1 Sample digestion. Digestion of geological and biological samples was performed in duplicate. About 100 mg of geological reference materials were weighed into 15 mL PFA vials (Savillex), followed by the addition of 3 mL of double-subboiled nitric acid, 2 mL of double-subboiled hydrochloric acid, 1 mL of hydrofluoric acid and 75 μL of hydrogen peroxide. The samples were digested for 48 hours at 130 °C on a hot plate (AHF analysentechnik AG, Tübingen, Germany). The digested samples were evaporated to dryness on the hot plate and redissolved in 2 mL of diluted boric acid to complex remaining hydrofluoric acid. After digestion, the solutions were transferred quantitatively to a pre-cleaned 50 mL DigiTUBE (SCP Science) and diluted to a final volume of 50 mL with HQ water.

Table 1 Protocol for the Sr purification procedure using Sr resin ($V = 500$ μL, Eichrom Technologies) and a peristaltic pump

Purification step	Reagent	Volume (mL)	Flow rate (μL min^{-1})
Pre-cleaning	5 mol L^{-1} HNO_3	3	1000
Pre-cleaning	HQ water	3	1000
Pre-cleaning	6 mol L^{-1} HCl	3	1000
Pre-cleaning	HQ water	3	1000
Conditioning	8 mol L^{-1} HNO_3	3	1000
Sample load	8 mol L^{-1} HNO_3	1.5	500
Matrix wash	8 mol L^{-1} HNO_3	10	1000
Sr elution	HQ water	5	500

About 100 mg of biological reference materials were weighted into 15 mL PFA vials (Savillex) and followed by the addition of 5 mL double-subboiled nitric acid and 0.5 mL of hydrogen peroxide. The samples were digested for 2 hours at 150 °C on a hot plate (AHF analysentechnik AG). After digestion, the solutions were transferred quantitatively to pre-cleaned 50 mL DigiTUBE (SCP Science) and diluted to a final volume of 15 mL with HQ water.

Analyte recoveries in the digests were found to be quantitative throughout all experiments, and consequently, complete digestion is assumed. Aliquots of each digest containing 1000 ng Sr were transferred to pre-cleaned 15 mL PFA vials (Savillex), evaporated at 80 °C to dryness, and redissolved in 1 mL of 8 mol L^{-1} nitric acid for subsequent purification.

2.3.2 Sr purification procedure. Approximately 500 μL of soaked Sr resin (Eichrom Technologies) was sandwiched between two frits in a 1 mL empty cartridge. The cartridge was connected to pump tubing as described elsewhere.[40] Reagents were pumped through the cartridge at a flow rate of 500 μL min^{-1} to 1000 μL min^{-1} using a peristaltic pump (MCP, ISMATEC, Barrington, IL, USA).

Purification was performed according to the standard protocol[41] with modifications as described in Table 1. In brief, Sr from the sample was loaded in 8 mol L^{-1} nitric acid onto the Sr resin while interferences (*i.e.*, Rb) and matrix elements (*e.g.*, Mg, Ca, K, and Fe) were not retained under these conditions and were washed off during rinsing with 8 mol L^{-1} nitric acid. Finally, Sr was eluted in HQ water. In accordance with previous studies,[41] the purification was repeated to minimize the impact of interferences and matrix elements. The purified Sr fractions were collected in pre-cleaned PFA vials and evaporated to dryness at 80 °C. To remove any remaining organic materials from the column, the residue was redissolved in 100 μL of concentrated nitric acid and 10 μL of hydrogen peroxide and evaporated to dryness at 80 °C again. For Sr isotopic analysis, the residue was redissolved in diluted nitric acid ($w(HNO_3) = 2\%$). Sr recovery was estimated based on MC-MICAP-MS measurements and was found to be greater than 75%, which is considered sufficient, as previous studies have demonstrated the absence of on-column Sr isotopic fractionation when using Sr resin (aka Sr Spec).[42]

2.3.3 Sr isotopic measurement routine, data processing, and uncertainty budget. Sr isotope abundance analyses were performed using the new MC-MICAP-MS instrument with N_2 (99.999% purity) as plasma gas. The instrument was coupled to an MicroDX autosampler (Elemental Scientific (ESI), Omaha, NE, USA) and equipped either with a PFA spray chamber (ESI) or an APEX Q high sensitivity sample introduction system (ESI), both in combination with a PFA nebulizer (ESI). The MC-MICAP-MS instrument was optimized daily using NIST SRM 987 solution for maximum intensity, signal stability, and peak shape. The torch position was manually adjusted using the *XYZ* stage, the gas flows were optimized using Radom MICAP-MS software, and the source lenses and ion transmission were optimized using Neptune software. All measurements were performed in low resolution mode after a minimum warm-up time of 30 minutes. General instrumental settings for the Sr isotope abundance measurements are described in Table 2.

The standard solution (*i.e.*, NIST SRM 987) and the samples were introduced into the plasma in the following sequence:

Table 2 Instrumental settings of the MC-MICAP-MS used for Sr isotope abundance ratio measurements

Parameter	MICAP ion source (Radom Instruments LLC)
Coolant gas (L min^{-1})	14
Auxiliary gas (L min^{-1})	1.1
Nebulizer gas (L min^{-1})	1.40–1.55
Power (W)	1500
Sampling depth (mm)	2 mm
Sample introduction	APEX Q (Elemental Scientific)
Nebulizer	PFA – 100 μL min^{-1} (Elemental Scientific)
Parameter	**MC-MS (Neptune, Thermo Fisher Scientific)**
Interface	Ni skimmer + sampler
Measured m/z	84 (Sr^+), 85 (Rb^+), 86 (Sr^+), 87 (Sr^+, Rb^+), 88 (Sr^+)
Center mass	$^{86}Sr^+$
Cup configuration	L2: 84, L1: 85, C: 86, H1: 87, H2: 88
Resolution	Low ($(m/z)/\Delta(m/z) \leq 400$)
Zoom optics – focus (V)	0.0
Zoom optics – dispersion (V)	0.0
Integration time (s)	4.2
Cycles/block	25
# of blocks	3–5
Sensitivity (V (μg g^{-1})$^{-1}$)	Approx. 40

standard1–sample–standard2, to enable correction for IIF *via* classical standard-sample bracketing (SSB).[1,18] Concentrations of the SSB standard solution and samples were matched within 15%, by adjusting the Sr mass concentration of the samples to either 300 ng mL^{-1} or 500 ng mL^{-1}. Data collection was accomplished with a total of 50–75 measurements per sample with an integration time of 4.2 s. The analytical and procedural blanks were negligible with a contribution of 0.02% and 0.1%, respectively. Therefore, no blank correction was performed for the measured data.

The conventional $^{87}Sr/^{86}Sr$ isotope abundance ratio (with the quantity symbol $R_{con}(^{87}Sr/^{86}Sr)$), which is corrected for IIF by internal normalization, was calculated according to internationally agreed-upon guidelines:[43] Residual ^{87}Rb interference was corrected *via* peak stripping of the simultaneously measured ^{85}Rb signal and using the natural $^{87}Rb/^{85}Rb$ isotope abundance ratio (=0.3856) recommended by IUPAC/CIAAW,[44,45] which was corrected for IIF using the conventional $^{88}Sr/^{86}Sr$ isotope abundance ratio. The measured $^{87}Sr/^{86}Sr$ isotope ratios were corrected for IIF by applying an IIF correction factor f which was obtained from the measured $^{88}Sr/^{86}Sr$ isotope abundance ratio and the conventional $^{88}Sr/^{86}Sr$ isotope abundance ratio defined as 8.375209 by using the exponential law. A constant IIF correction factor f was assumed for both $^{88}Sr/^{86}Sr$ and $^{87}Sr/^{86}Sr$ isotope abundance ratios. The commonly accepted value for the conventional $^{87}Sr/^{86}Sr$ isotope abundance ratio of NIST SRM 987 is 0.710250.[43] Furthermore, after correction for Rb as described above, dimensionless $\delta^{87}Sr/^{86}Sr_{SRM987}$ and $\delta^{88}Sr/^{86}Sr_{SRM987}$ values (in ‰) were calculated relative to the average isotope abundance ratios of NIST SRM 987 used as the bracketing standard, following the classical SSB approach.[1,18]

The measurement uncertainty for the conventional $^{87}Sr/^{86}Sr$ isotope abundance ratio was estimated based on the precision of the measurement (*i.e.*, standard error of the mean) and the repeatability of the SSB standard (*i.e.*, $R_{con}(^{87}Sr/^{86}Sr)$ value). The measurement uncertainty of the $\delta^{87}Sr/^{86}Sr_{SRM987}$ and $\delta^{88}Sr/^{86}Sr_{SRM987}$ values was estimated based on the precision of the measurement (*i.e.*, standard deviation) and the variability of the NIST SRM 987 standard in the bracket.

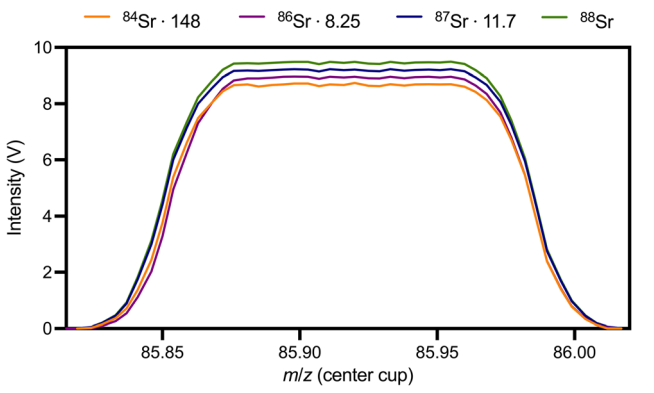

Fig. 2 Mass scan of 300 ng mL^{-1} NIST SRM 987 solution in low resolution mode. Sample introduction using APEX Q (wet plasma).

3. Results and discussion

3.1. Peak shape, sensitivity and isotope ratio precision

The MC-MICAP-MS instrument showed highly stable signals and produced flat-topped, symmetrical peak shapes in low resolution mode with both wet sample introduction and dry sample introduction (see Fig. 2). This confirms that the double-focusing properties of the Neptune platform were sustained and fully functional with the MICAP ion source, a very promising prerequisite for high-precision isotope abundance measurements.

MC-MICAP-MS with wet sample introduction (*i.e.*, PFA spray chamber) yielded a sensitivity of approx. 10 V $(\mu g\ g^{-1})^{-1}$. When using the Ar-ICP as the ion source, our Neptune platform achieved a sensitivity of 25 V $(\mu g\ g^{-1})^{-1}$. Notably, our Neptune (installed 2009) was specified under wet plasma conditions with a sensitivity for ^{88}Sr of >20 V $(\mu g\ g^{-1})^{-1}$. The sensitivity of MC-MICAP-MS is therefore lower by a factor of about 2.5 compared to MC-ICP-MS. This agrees well with observations from elemental analysis using MICAP-MS reporting a reduction in sensitivity by a factor of 2 as compared to ICP-MS.[33] Dry sample introduction (*i.e.*, APEX Q without a membrane) on the MC-MICAP-MS lead to a higher sensitivity of approx. 40 V $(\mu g\ g^{-1})^{-1}$. This improvement in sensitivity by a factor of 4 is consistent with observations from the Neptune using Ar-ICP as the ion source with the same dry sample introduction. Furthermore, elemental analysis using MICAP-MS reported signal enhancement by a factor of 5 to 10 when using the same dry sample introduction.[33,46] Given the gain in sensitivity through dry sample introduction, most of the assessments presented below, as well as the measurements of geological and biological reference materials, were performed using an Apex Q desolvating nebulizer.

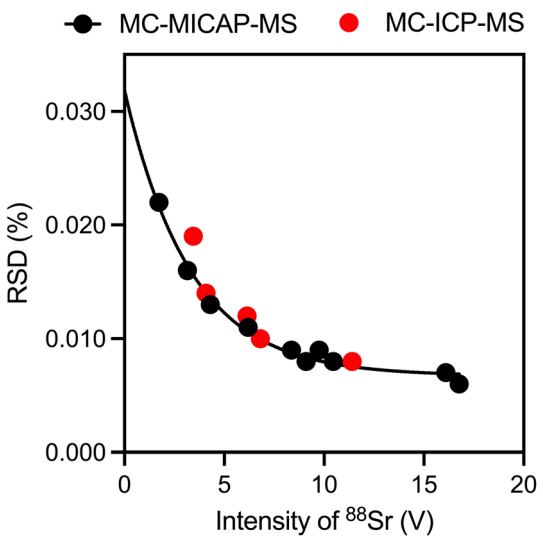

Fig. 3 Comparison of $^{87}Sr/^{86}Sr$ intensity ratio precision, expressed as RSD (%), between MC-MICAP-MS and MC-ICP-MS (Ar-Neptune). Data collection: 75 runs at an integration time of 4.2 s.

At an intensity of 16.5 V on $^{88}Sr^{+}$ (*i.e.*, 500 ng mL^{-1}), the $^{87}Sr/^{86}Sr$ intensity ratio precision was approx. 0.007% for MC-MICAP-MS. Fig. 3 shows good agreement in the $^{87}Sr/^{86}Sr$ intensity ratio precision at various intensities between the MC-MICAP-MS and our Neptune platform using Ar-ICP as the ion source. This good agreement was expected and can be explained by the fact that the main features of multi-collector mass spectrometers for high-precision isotope abundance measurements, *i.e.*, flat-topped peaks and simultaneous ion detection, were preserved in the new MC-MICAP-MS instrument.

3.2. IIF per mass unit and stability of IIF

For MC-ICP-MS, it is known that the magnitude of IIF changes from element to element: The IIF per mass unit usually ranges from 0.5–1.5% for heavier elements (*e.g.*, Pb and U) and up to 25% for lighter elements (*e.g.*, Li and B).[1,14,15] Here, an IIF per mass unit of approx. 16% for B, approx. 2.1% for Sr, and approx. 0.90% for Pb is reported for the MC-MICAP-MS instrument. These values agree well with those observed for our Neptune platform using Ar-ICP as the ion source; with approx. 13% for B, approx. 2.0% for Sr, and approx. 0.80% for Pb. Therefore, the extent and algebraic sign (direction) of IIF per mass unit observed for B, Sr, and Pb when using MICAP as the ion source is comparable to those observed for the same elements when using Ar-ICP as the ion source.

For Sr on the MC-MICAP-MS, the IIF per mass unit values for the $^{87}Sr/^{86}Sr$ and $^{88}Sr/^{86}Sr$ intensity ratios were 2.07% ± 0.13% (2 SD) and 2.03% ± 0.12% (2 SD) for 93 discontinuous measurements of NIST SRM 987 over seven days of measurement. This indicates that the two isotope pairs of Sr have very similar IIF per mass unit values. Again, this agrees well with observations from the Neptune platform using Ar-ICP as the ion source; with IIF per mass unit values of 2.03% ± 0.17% (2 SD) and 1.99% ± 0.16% (2 SD) for $^{87}Sr/^{86}Sr$ and $^{88}Sr/^{86}Sr$ intensity ratios, respectively, based on 28 discontinuous measurements of NIST SRM 987 over four days of measurement. Furthermore, the day-to-day stability of the IIF per mass unit observed for Sr using MICAP as the ion source is comparable to the between-day stability of the IIF per mass unit value observed for the same element using Ar-ICP as the ion source.

For MC-ICP-MS it is known that IIF drifts over time.[1] Fluctuations in IIF throughout a sequence present a significant hindrance to the determination of reliable and precise isotope abundance ratios, and must be addressed through an appropriate IIF correction strategy.[14,17] Here, a repeatability of 0.010% for the $^{87}Sr/^{86}Sr$ intensity ratio was observed for 21 measurements of NIST SRM 987 over a nine-hour measurement period for MC-MICAP-MS with wet sample introduction. When comparing the maximum to the minimum of the measured $^{87}Sr/^{86}Sr$ intensity ratios (2.5 hours apart), the difference is a δ-value of 0.31‰. For MC-MICAP-MS with dry sample introduction, a repeatability of 0.009% for the $^{87}Sr/^{86}Sr$ intensity ratio was observed for 20 measurements of NIST SRM 987 over a five-hour measurement period, with a δ-value of 0.35‰ when comparing the maximum to the minimum of the measured $^{87}Sr/^{86}Sr$ intensity ratios (4.5 hours apart). For the Neptune platform using Ar-ICP as the ion source, a repeatability of 0.012% for the $^{87}Sr/^{86}Sr$ intensity ratio was observed for 21 measurements of NIST SRM 987 over a nine-hour measurement period. When comparing the maximum to the minimum of the measured $^{87}Sr/^{86}Sr$ intensity ratios (4 hours apart), the difference is a δ-value of 0.45‰. Consequently, the long-term stability of IIF for Sr when using MICAP as the ion source is comparable to the long-term stability of IIF observed for the same element when using Ar-ICP as the ion source. Constant IIF is an important prerequisite for the successful application of IIF correction strategies such as SSB and combined SSB and internal normalization (C-SSBIN), which are based on sequential measurements of standards and samples.

3.3. Effect of plasma conditions on IIF

For MC-ICP-MS, it was found that plasma conditions such as radial (*i.e.*, *x*-, *y*-position) and axial (*i.e.*, *z*-position) plasma sampling positions, as well as nebulizer gas flow and RF plasma power had significant effects on the magnitude of IIF.[1,47]

Fig. 4 shows the $\delta^{87}Sr/^{86}Sr_{SRM987}$ values and $^{88}Sr^{+}$ intensities as a function of the radial torch position (*i.e.*, *x*- and *y*-position) relative to the optimum position (defined as 0 mm) for MC-MICAP-MS. The intensity distribution is symmetrical around the center of the plasma, decreasing to approx. 25% of the maximum at a *x*-position of 0.7 mm and a *y*-position of 0.5 mm. This trend agrees with previous observations for MC-ICP-MS. The distribution of $^{87}Sr/^{86}Sr$ isotope abundance ratios (expressed as δ-values) is symmetrical around the center of the plasma, increasing to approx. 0.45‰ at a *x*-position of 0.7 mm (see Fig. 4A) and approx. 0.7–1.0‰ at a *y*-position of 0.5 mm (see Fig. 4B); indicating that the lighter ^{86}Sr isotope is more efficiently sampled at the center of the plasma of MC-MICAP-MS then towards the edges. The center of the plasma has a radial area of approx. 0.02 mm^2 with stable $^{88}Sr^{+}$ signal intensity and stable IIF. The observed IIF behaviour can be explained by the "zone-model" for Ar-ICP as proposed by Vanhaecke *et al.*:[48] Assuming that the zone with maximum analyte density coincides with the center of the plasma, and given the higher dispersal rates for lighter isotopes, the $^{87}Sr/^{86}Sr$ intensity ratio would be expected to display a minimum at the center while increasing towards edges of the analytical zone.[47] The general trend of increasing $^{87}Sr/^{86}Sr$ isotope abundance ratios with increasing distance to the center of the plasma of MC-MICAP-MS agrees with previous observations for MC-ICP-MS.[47] However, previous studies have reported a bimodal heavy-to-light isotope abundance ratio profile for MC-ICP-MS,[47] that is not seen for MC-MICAP-MS.

Fig. 5 shows the $\delta^{87}Sr/^{86}Sr_{SRM987}$ values and $^{88}Sr^{+}$ intensities as a function of sampling depth (*i.e.*, *z*-position, nebulizer gas flow) relative to the optimum position (*i.e.*, 2 mm and 1.55 L min^{-1}) for MC-MICAP-MS. The intensity distribution remains reasonably stable with increasing sampling distance until a *z*-position of approx. 2.9 mm, while the intensity decreases with decreasing nebulizer gas flow. The $^{87}Sr/^{86}Sr$ isotope abundance ratio (expressed as δ-values) increases with increasing sampling distance, with a maximum of approx. 0.4‰ at a *z*-position of

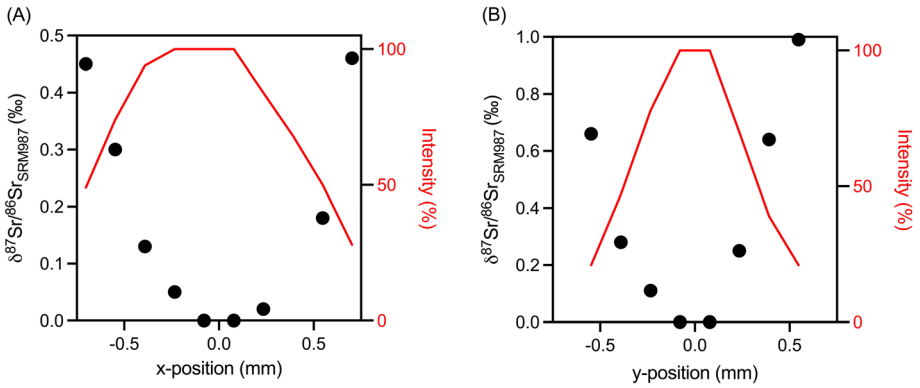

Fig. 4 $\delta^{87}Sr/^{86}Sr_{SRM987}$ and $^{88}Sr^{+}$ intensity as a function of (A) *x*-position and (B) *y*-position of the torch relative to the optimum position (defined as 0 mm). Measurement precision (1 SD) ranges from 0.10‰ to 0.25‰ for the $\delta^{87}Sr/^{86}Sr_{SRM987}$ values and from 0.5% to 5.0% for the $^{88}Sr^{+}$ intensities (see Fig. S1). For improved readability, no error bars are shown in the figures.

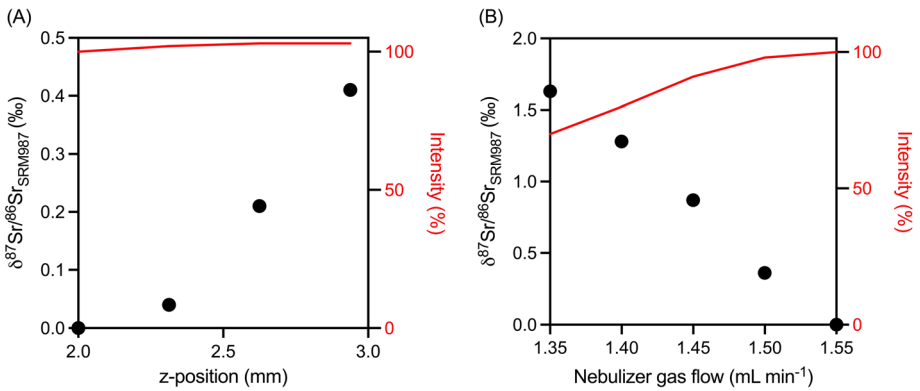

Fig. 5 (A) $\delta^{87}Sr/^{86}Sr_{SRM987}$ and $^{88}Sr^{+}$ intensity as a function of *z*-position of the torch relative to the optimum position of 2 mm. (B) $\delta^{87}Sr/^{86}Sr_{SRM987}$ and $^{88}Sr^{+}$ intensity as a function of nebulizer gas flow relative to the optimum flow of 1.55 L min^{-1}. Measurement precision (1 SD) is about 0.09‰ for the $\delta^{87}Sr/^{86}Sr_{SRM987}$ values and ranges from 1.0% to 4.0% for the $^{88}Sr^{+}$ intensities (see Fig. S2). For improved readability, no error bars are shown in the figures.

approx. 2.9 mm (see Fig. 5A), as well as with decreasing nebulizer flow, with a maximum of approx. 1.6‰ at a nebulizer flow of 1.35 L min^{-1} (see Fig. 5B). This indicates that the lighter ^{86}Sr isotope is more efficiently sampled when the torch is close to the cones and/or the nebulizer gas flow is high for the MC-MICAP-MS. The observed IIF behaviour can be explained as a consequence of the "zone-model" for Ar-ICP as proposed by Vanhaecke *et al.*[48] indicating that lighter isotopes should show maximum density and intensity lower in the plasma, *i.e.*, closer to the torch or at higher nebulizer gas flows.[47] Hence, $^{87}Sr/^{86}Sr$ isotope abundance ratios should increase with decreasing sampling depth, *e.g.*, by moving the torch away from the sampler cone or decreasing the nebulizer gas flow.[47,48] For MC-ICP-MS, previous studies reported far more complicated dependence on sampling depth.[47]

Fig. 6 shows the $\delta^{87}Sr/^{86}Sr_{SRM987}$ values and $^{88}Sr^{+}$ intensities as a function of decreasing microwave plasma power relative to the optimum position (*i.e.*, 1500 W) for MC-MICAP-MS. Previous studies using MICAP-MS reported stable operation of the plasma for powers between 1100 and 1500 W.[33] The intensity distribution remains fairly stable with decreasing plasma power reaching the minimum tested value of 1200 W for MC-MICAP-MS. The $^{87}Sr/^{86}Sr$ isotope abundance ratio (expressed as δ-values) decreases with decreasing plasma power, with a minimum of approx. −4.7‰ at 1200 W; showing the most significant impact on the IIF behaviour of MC-MICAP-MS. The observed trend indicates that the lighter ^{86}Sr isotope is more efficiently sampled with lower plasma power of MC-MICAP-MS. Consistent with observations of the nebulizer gas flow effect, the influence of plasma power on Sr isotope abundance ratios in the MICAP appears to be correlated with the preferential diffusion of lighter isotopes at higher temperatures (*i.e.*, high microwave plasma power and/or low nebulizer gas flow). The observed trend in IIF behaviour related to the plasma power of the MICAP does not agree with the trends observed for Ar-ICP, where the heavy-to-light isotope abundance ratios increase with decreasing RF plasma power.[49] The explanation for these opposing trends in terms of plasma power and IIF between MC-MICAP-MS and MC-ICP-MS is unclear, but is likely linked to the differences in the generation of the inductive field that transfers

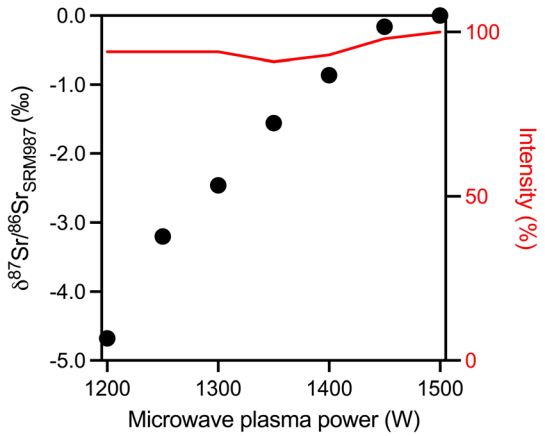

Fig. 6 $\delta^{87}Sr/^{86}Sr_{SRM987}$ and $^{88}Sr^{+}$ intensity as a function of plasma power relative to the optimum power of 1500 W. Measurement precision (1 SD) is about 0.14‰ for the $\delta^{87}Sr/^{86}Sr_{SRM987}$ values and ranges from 1.5% to 2.5% for the $^{88}Sr^{+}$ intensities (see Fig. S3). For improved readability, no error bars are shown in the figure.

power to the plasma. Nevertheless, the ability to induce IIF by changing the plasma power is an important prerequisite for the successful application of IIF correction strategies such as the optimized regression model[1] (ORM, aka empirical external normalization (EEN) model).

3.4. Nature of IIF and common correction strategies

The nature of isotope fractionation in MC-MICAP-MS is evaluated and ascertained by using a simplified three-isotope-plot of natural logarithms of measured $^{88}Sr/^{86}Sr$ and $^{87}Sr/^{86}Sr$ isotope intensity ratios (see Fig. 7). If the underlying mechanism of the isotope fractionation process is mass-dependent, the slope of this plot can be predicted from the nuclide masses alone and the three-isotope-plot exhibits behavior consistent with empirical mass-dependent fractionation models.[1,11] Since the 1990s, numerous conventional isotopic fractionation models (*e.g.*, the linear law, the power law, and the exponential law), originally developed for TIMS, have been conveniently adapted for MC-ICP-MS, with the exponential law of Russell *et al.*[50] being the most widely used.[1,17,18] As MICAP is an atmospheric-pressure inductively coupled plasma source similar to conventional Ar-ICP, it is reasonable to expect that the adapted isotope fractionation models apply as well.

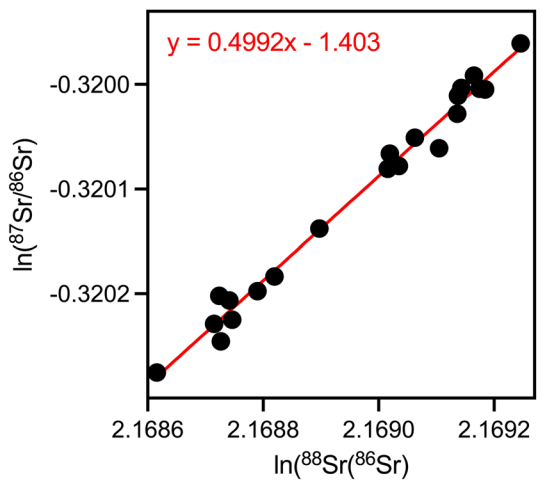

Fig. 7 Three-isotope plot of Sr from 21 measurements ($N = 75$ runs) of NIST SRM 987 over 9 hours.

The three-isotope-plot in Fig. 7 shows a linear correlation of the data with a slope of 0.499 ± 0.013 which overlaps with the slope calculated using the empirical Russell law (exponential law) of 0.503. It can be therefore concluded that MC-MICAP-MS exhibits predominantly mass-dependent isotope fractionation behavior for Sr. This is an important prerequisite for the successful application of IIF correction strategies that rely on mass-dependent fractionation models such as internal normalization and double spike. However, the presence of potential mass-independent fractionation in MC-MICAP-MS measurements cannot not be excluded at this point. The nature of IIF, its behaviour and its stability throughout the measurement have a significant impact on the choice of the IIF correction model to determine reliable isotope ratios.[1]

The conventional $^{87}Sr/^{86}Sr$ isotope abundance ratio is commonly reported as a result from MC-ICP-MS and TIMS measurements. These data are corrected for IIF by internal normalization using the conventional $^{88}Sr/^{86}Sr$ isotope abundance ratio (=8.375209) according to empirical mass-dependent fractionation models. The conventional $^{87}Sr/^{86}Sr$ isotope abundance ratio of NIST SRM 987 determined by MC-MICAP-MS over five measurement days is 0.710256 ± 0.000018 (2 SD, $N = 70$). This agrees well with the commonly accepted value for the conventional $^{87}Sr/^{86}Sr$ isotope abundance ratio for NIST SRM 987 (=0.710250 ± 0.000001 (ref. 43)), obtained by either TIMS or MC-ICP-MS. Furthermore, the intermediate precision for the conventional $^{87}Sr/^{86}Sr$ isotope abundance ratio of NIST SRM 987 obtained by MC-MICAP-MS is 0.0013% ($N = 70$) which agrees well with our observations from the Neptune using Ar-ICP as the ion source showing a similar intermediate precision of ≈0.0020%. Overall, this indicates both reliability and repeatability for the determination of the conventional $^{87}Sr/^{86}Sr$ isotope abundance ratio obtained by MC-MICAP-MS and the applicability of internal normalization as an IIF correction strategy.

In general, the applicability of internal normalization as an IIF correction strategy for $^{87}Sr/^{86}Sr$ isotope abundance ratios is limited for two reasons: (1) it is built on the assumption that the $^{88}Sr/^{86}Sr$ isotope abundance ratio is constant (studies have revealed that this is not the case, and $^{88}Sr/^{86}Sr$ isotope abundance ratios vary in nature[51–53]). (2) If mass-independent fractionation is present, as shown for Sr isotope abundance ratios obtained by MC-ICP-MS,[41] biased results may occur when mass-dependent fractionation models, *e.g.*, exponential law, are used for IIF correction. The SSB technique has been used as an alternative IIF correction strategy for Sr due to its simplicity, its capability to correct for both mass-dependent and mass-independent fractionation, and the possibility to determine $\delta^{88}Sr/^{86}Sr_{SRM987}$ values by MC-ICP-MS.[1,41] Over five measurement days, NIST SRM 987 was repeatedly measured against

Table 3 Conventional $^{87}Sr/^{86}Sr$ isotope abundance ratios as well as $\delta^{87}Sr/^{86}Sr_{SRM987}$ and $\delta^{88}Sr/^{86}Sr_{SRM987}$ values for duplicate digests of the geological and biological reference material. Errors were considered equal to the expanded uncertainty (U, $k = 2$)

Reference material	$R_{con}(^{87}Sr/^{86}Sr)$ value – this study	Published $R_{con}(^{87}Sr/^{86}Sr)$ value	$\delta^{87}Sr/^{86}Sr_{SRM987}$ value – this study (‰)	Published $\delta^{87}Sr/^{86}Sr_{SRM987}$ value (‰)	$\delta^{88}Sr/^{86}Sr_{SRM987}$ value – this study (‰)	Published $\delta^{88}Sr/^{86}Sr_{SRM987}$ value (‰)
IAPSO (seawater)	0.709168 ± 0.000022	0.709178 ± 0.000013 (ref. 55)[a]	−1.33 ± 0.14	−1.44 ± 0.10 (ref. 43)[c]	0.39 ± 0.12	0.36 ± 0.03 (ref. 56)
	0.709159 ± 0.000021		−1.35 ± 0.12		0.38 ± 0.12	0.38 ± 0.01 (ref. 55)[a]
BCR-2 (basalt)	0.705004 ± 0.000023	0.705012 ± 0.000014 (ref. 55)[a]	−7.22 ± 0.18	−7.38 ± 0.04 (ref. 57)[c]	0.31 ± 0.09	0.22 + 0.07 (ref. 56)
	0.705018 ± 0.000022		−7.22 ± 0.18		0.29 ± 0.13	0.25 ± 0.02 (ref. 58)
OU6 (slate)	0.729758 ± 0.000022	0.729778 ± 0.000047 (ref. 43)	27.60 ± 0.15	27.49 ± 0.06 (ref. 43)[c]	0.28 ± 0.12	—
	0.729777 ± 0.000013		27.51 ± 0.28	27.59 ± 0.19 (ref. 43)[d]		
NIST SRM 1400 (bone ash)	0.713123 ± 0.000014	0.713129 ± 0.000019 (ref. 56)	3.88 ± 0.13	3.93 ± 0.03 (ref. 56)	−0.30 ± 0.09	−0.32 ± 0.03 (ref. 56)
	0.713118 ± 0.000014		3.87 ± 0.13	3.87 ± 0.23 (ref. 59)	−0.28 ± 0.10	−0.33 ± 0.02 (ref. 58)
NIST SRM 1486 (bone meal)	0.709326 ± 0.000014	0.709309 ± 0.000011 (ref. 55)[b]	−1.50 ± 0.15	−1.37 ± 0.08 (ref. 60)[c]	−0.36 ± 0.10	−0.37 ± 0.02 (ref. 58)
	0.709322 ± 0.000013		−1.51 ± 0.14	−1.59 ± 0.22 (ref. 61 and 62)[d]	−0.38 ± 0.13	

[a] Reference values are obtained as median from the data provided in the GeoReM database on June 27th, 2025. [b] Reference values are obtained as median from the data provided in the GeoReM database on June 27th, 2025, excluding data from LA-MC-ICP-MS. [c] $\delta^{88}Sr/^{86}Sr_{SRM987}$ value was calculated based on reported $\delta^{87}Sr/^{86}Sr$ isotope abundance ratios for samples and NIST SRM 987. [d] Reference value was calculated based on the mean of replicate analyses of the sample, carried out by the authors as part of the studies.

Fig. 8 Correlation between conventional $^{87}Sr/^{86}Sr$ isotope abundance ratios of geological and biological reference materials measured by MC-MICAP-MS and their reported conventional values in the literature (see Table 3). The error bars are smaller than the data points shown in the figure.

itself using the classical SSB approach. The resulting $\delta^{87}Sr/^{86}Sr_{SRM987}$ and $\delta^{88}Sr/^{86}Sr_{SRM987}$ values are reported as 0.00‰ ± 0.03‰ (2 SD, $N = 17$) and 0.00‰ ± 0.04‰ (2 SD, $N = 17$), respectively. These results demonstrate that the IIF behaviour is sufficiently stable to enable the reliable application of the SSB approach in MC-MICAP-MS measurements. Furthermore, the intermediate precision of the $\delta^{87}Sr/^{86}Sr_{SRM987}$ and $\delta^{88}Sr/^{86}Sr_{SRM987}$ values is comparable to that reported for MC-ICP-MS measurements.[54] Given the consistent and stable IIF behaviour of the MC-MICAP-MS instrument, the SSB approach represents a suitable IIF correction strategy for obtaining reliable and precise $\delta^{87}Sr/^{86}Sr_{SRM987}$ and $\delta^{88}Sr/^{86}Sr_{SRM987}$ values.

3.5. Sr isotopic composition of reference materials

Finally, the accuracy of the Sr isotope abundance measurements using MC-MICAP-MS was validated by measuring three geological reference materials (*i.e.*, IAPSO, BCR-2, and OU6) and two biological reference materials (*i.e.*, NIST SRM 1400 and NIST SRM 1486) which were previously analyzed for their Sr isotopic composition using either MC-ICP-MS or TIMS.

In Table 3, the conventional $^{87}Sr/^{86}Sr$ isotope abundance ratio, the $\delta^{87}Sr/^{86}Sr_{SRM987}$ values, and the $\delta^{88}Sr/^{86}Sr_{SRM987}$ values of the different geological and biological reference materials are reported and compared to data obtained from previous studies. Overall, the values reported in the present study for the five reference materials overlap within uncertainty with previously reported data. The repeatability of the conventional $^{87}Sr/^{86}Sr$ isotope abundance ratios is <0.002% (RSD), and that of the $\delta^{88}Sr/^{86}Sr_{SRM987}$ values is <0.05‰ (2 SD) for duplicate digests of the geological and biological reference materials.

Additionally, the conventional $^{87}Sr/^{86}Sr$ isotope abundance ratios obtained by MC-MICAP-MS for the geological and

biological reference materials are compared to literature values in Fig. 8. All data points fall on the 1 : 1 line, indicating consistency between the conventional $^{87}Sr/^{86}Sr$ isotope abundance ratios obtained by MC-MICAP-MS and both previous MC-ICP-MS and TIMS results. Overall, the conventional $^{87}Sr/^{86}Sr$ isotope abundance ratios as well as the $\delta^{87}Sr/^{86}Sr_{SRM987}$ and the $\delta^{88}Sr/^{86}Sr_{SRM987}$ values obtained with MC-MICAP-MS are consistent with data previously obtained by either TIMS or MC-ICP-MS (standard bracketing and double spike), demonstrating the accuracy of the new MC-MICAP-MS instrument.

4. Conclusion

The MC-MICAP-MS instrument is a promising new development in multi-collector mass spectrometry used for high-precision isotope abundance ratio measurements. In direct comparison to MC-ICP-MS, the sensitivity of the new MC-MICAP-MS instrument for Sr is lower; as it was to be expected from previous observations in elemental analysis using MICAP-MS. Initial investigations on Sr showed that the new MC-MICAP-MS instrument is fully comparable to conventional MC-ICP-MS systems in terms of intensity ratio precision (approx. 0.007%), repeatability of intensity ratios (approx. 0.010%), and intermediate precision for isotope abundance ratios. In addition, the investigations showed that the IIF behaviour of the new MC-MICAP-MS is predominantly mass-dependent for Sr and that common IIF correction strategies such as internal normalization and SSB can be successfully applied; demonstrating high reliability for Sr isotope abundance ratio measurements. Finally, the consistency in the conventional $^{87}Sr/^{86}Sr$ isotope abundance ratios obtained by MC-MICAP-MS with previous results obtained using established technology (*i.e.*, MC-ICP-MS and TIMS) confirmed the accuracy of measurements performed with the new MC-MICAP-MS. Overall, these experimental results demonstrate that MICAP can be used as an alternative ion source for a multi-collector mass spectrometer without compromising its double-focusing and high-precision properties or the accuracy and reliability of the measurement results. This agrees well with observations by Lin *et al.*[32] showing similar success when replacing the ICP of a multi-collector mass spectrometer with a low-pressure He-MIP.

Work is continuing to improve the new instrument, *e.g.*, by implementing a high sensitivity interface through an additional vacuum pump and different cones (*i.e.*, material and orifice). Furthermore, the applicability of other IIF correction strategies, like C-SSBIN, the optimized regression model and double spike, as well as the impact of matrix effects requires systematic investigation in the future. With a wealth of potential applications, including K, Ca, Fe, and Se, significant further work will be required to fully explore the potential of the new technology for the isotope research community.

Author contributions

AR: conceptualization, methodology, investigation, validation, writing – original draft, visualization, project administration. AM: methodology, writing – review & editing. MEW: investigation, resources, writing – review & editing.

Conflicts of interest

AM is the CEO and founder of Radom Instruments LLC. The remaining authors declare that no conflict of interest exists.

Data availability

Data will be made available on request.

Supplementary information is available and includes supplementary plots related to Fig. 4–6. See DOI: **https://doi.org/10.1039/d5ja00271k**.

Acknowledgements

AR is funded by the Leopoldina Postdoc Scholarship (LPDS 2022-14) from the German National Academy of Sciences. MEW is supported by an NSERC Discovery Grant. The authors would like to thank the Department of Physics and Astronomy and the Faculty of Science at University of Calgary for the financial support. Furthermore, the authors would also like to thank Peter Stow from Isomass Scientific Inc. for his support. Finally, the authors would like to thank Kerri Miller and Behnam Ashrafkhani for their help in the lab and during the installation of the MICAP ion source.

References

1 L. Yang, S. Tong, L. Zhou, Z. Hu, Z. Mester and J. Meija, *J. Anal. At. Spectrom.*, 2018, **33**, 1849–1861.
2 J. G. Wiederhold, *Environ. Sci. Technol.*, 2015, **49**, 2606–2624.
3 A. G. Nord and K. Billström, *Heritage Sci.*, 2018, **6**, 25–37.
4 J. A. Stephens, M. N. Ducea, D. J. Killick and J. Ruiz, *J. Archaeol. Sci.*, 2021, **127**, 105334.
5 J. Irrgeher, D. Bandoniene, J. Draxler and T. Prohaska, Elemental and Isotopic Analyses in Forensic Sciences, *Encyclopedia of Analytical Chemistry*, ed. R. A. Meyers, John Wiley & Sons, 2020.
6 J. Irrgeher and T. Prohaska, *Anal. Bioanal. Chem.*, 2016, **408**, 369–385.
7 M. Wiggenhauser, R. E. T. Moore, P. Wang, G. P. Bienert, K. H. Laursen and S. Blotevogel, *Front. Plant Sci.*, 2022, **13**, 840941.
8 B. Mahan, R. S. Chung, D. L. Pountney, F. Moynier and S. Turner, *Cell. Mol. Life Sci.*, 2020, **77**, 3293–3309.
9 F. Vanhaecke and M. Costas-Rodríguez, *View*, 2020, **2**, 20200094.
10 A. J. Walder and P. A. Freedman, *J. Anal. At. Spectrom.*, 1992, **7**, 571–575.
11 M. Wieser, J. Schwieters and C. Douthitt, *Isot. Anal.*, 2012, 77–91, DOI: **10.1002/9783527650484.ch3**.
12 N. Jakubowski, M. Horsky, P. H. Roos, F. Vanhaecke and T. Prohaska, in *Sector Field Mass Spectrometry for Elemental and Isotopic Analysis*, The Royal Society of Chemistry, 2015, pp. 208–318.

13 T. Prohaska, in *Sector Field Mass Spectrometry for Elemental and Isotopic Analysis*, ed. T. Prohaska, J. Irrgeher, A. Zitek and N. Jakubowski, The Royal Society of Chemistry, 2015, pp. 121–125.
14 J. Meija, L. Yang, Z. Mester and R. E. Sturgeon, in *Isotopic Analysis*, Wiley-VCH Verlag GmbH & Co. KGaA, 2012, pp. 113–137, DOI: 10.1002/9783527650484.ch5.
15 J. Irrgeher and T. Prohaska, in *Sector Field Mass Spectrometry for Elemental and Isotopic Analysis*, ed. T. Prohaska, J. Irrgeher, A. Zitek and N. Jakubowski, The Royal Society of Chemistry, 2015, pp. 107–120.
16 F. Albarède, E. Albalat and P. Télouk, *J. Anal. At. Spectrom.*, 2015, **30**, 1736–1742.
17 L. Yang, *Mass Spectrom. Rev.*, 2009, **28**, 990–1011.
18 J. Irrgeher, J. Vogl, J. Santner and T. Prohaska, in *Sector Field Mass Spectrometry for Elemental and Isotopic Analysis*, ed. T. Prohaska, J. Irrgeher, A. Zitek and N. Jakubowski, The Royal Society of Chemistry, 2015, pp. 126–151.
19 K.-Y. Chen, H.-L. Yuan, P. Liang, Z.-A. Bao and L. Chen, *Int. J. Mass Spectrom.*, 2017, **421**, 196–203.
20 K. Hobin, M. Costas Rodriguez and F. Vanhaecke, *Anal. Chem.*, 2021, **93**, 8881–8888.
21 G. Craig, H. Wehrs, D. G. Bevan, M. Pfeifer, J. Lewis, C. D. Coath, T. Elliott, C. Huang, N. S. Lloyd and J. B. Schwieters, *Anal. Chem.*, 2021, **93**, 10519–10527.
22 W. Dai, F. Moynier, M. Paquet, J. Moureau, B. Debret, J. Siebert, Y. Gerard and Y. Zhao, *Chem. Geol.*, 2022, **590**, 120688.
23 B.-Y. Gao, B.-X. Su, W.-J. Li, M. Yuan, J. Sun, Y. Zhao and X. Liu, *J. Anal. At. Spectrom.*, 2022, **37**, 2111–2121.
24 A. J. Schwartz, Y. Cheung, J. Jevtic, V. Pikelja, A. Menon, S. J. Ray and G. M. Hieftje, *J. Anal. At. Spectrom.*, 2016, **31**, 440–449.
25 C. I. M. Beenakker, *Spectrochim. Acta, Part B*, 1976, **31**, 483–486.
26 J. Hubert, M. Moisan and A. Ricard, *Spectrochim. Acta, Part B*, 1979, **34**, 1–10.
27 M. Moisan, R. Pantel, J. Hubert, E. Bloyet, P. Leprince, J. Marec and A. Ricard, *J. Microwave Power*, 1979, **14**, 57–61.
28 Y. Okamoto, *J. Anal. At. Spectrom.*, 1994, **9**, 745–749.
29 M. Ohata and N. Furuta, *J. Anal. At. Spectrom.*, 1998, **13**, 447–453.
30 M. Ohata, H. Ota, M. Fushimi and N. Furuta, *Spectrochim. Acta, Part B*, 2000, **55**, 1551–1564.
31 M. R. Hammer, *Spectrochim. Acta, Part B*, 2008, **63**, 456–464.
32 J. Lin, Z. Liu, Y. Liu, W. Liu, X. Jiang, G. Zhao, L. Chen and Z. Hu, *Anal. Chem.*, 2023, **95**, 16877–16884.
33 M. Schild, A. Gundlach-Graham, A. Menon, J. Jevtic, V. Pikelja, M. Tanner, B. Hattendorf and D. Gunther, *Anal. Chem.*, 2018, **90**, 13443–13450.
34 C. Neff, P. Becker, B. Hattendorf and D. Gunther, *J. Anal. At. Spectrom.*, 2021, **36**, 1750–1757.
35 A. Winckelmann, J. Roik, S. Recknagel, C. Abad and Z. You, *J. Anal. At. Spectrom.*, 2023, **38**, 1253–1260.
36 Z. You, A. Akkuş, W. Weisheit, T. Giray, S. Penk, S. Buttler, S. Recknagel and C. Abad, *J. Anal. At. Spectrom.*, 2022, **37**, 2556–2562.
37 K. G. Heumann, S. M. Gallus, G. Rädlinger and J. Vogl, *J. Anal. At. Spectrom.*, 1998, **13**, 1001–1008.
38 A. Retzmann, S. Faßbender, M. Rosner, M. von der Au and J. Vogl, *J. Anal. At. Spectrom.*, 2023, **38**, 2144–2158.
39 W. A. Brand, T. B. Coplen, J. Vogl, M. Rosner and T. Prohaska, *Pure Appl. Chem.*, 2014, **86**, 425–467.
40 A. Retzmann, D. Walls, K. A. Miller, J. Irrgeher, T. Prohaska and M. E. Wieser, *Anal. Bioanal. Chem.*, 2022, **414**, 675–689.
41 J. Irrgeher, T. Prohaska, R. E. Sturgeon, Z. Mester and L. Yang, *Anal. Methods*, 2013, **5**, 1687.
42 D. De Muynck, G. Huelga-Suarez, L. Van Heghe, P. Degryse and F. Vanhaecke, *J. Anal. At. Spectrom.*, 2009, **24**, 1498.
43 A. Kazlagić, M. Rosner, A. Cipriani, D. A. Frick, J. Glodny, E. J. Hoffmann, J. M. Hora, J. Irrgeher, F. Lugli, T. Magna, T. C. Meisel, A. Meixner, A. Possolo, A. Pramann, M. J. Pribil, T. Prohaska, A. Retzmann, O. Rienitz, D. Rutherford, G. M. Paula-Santos, M. Tatzel, S. Widhalm, M. Willbold, T. Zuliani and J. Vogl, *Geostand. Geoanal. Res.*, 2023, **47**(4), 821–840.
44 T. Prohaska, J. Irrgeher, J. Benefield, J. K. Böhlke, L. A. Chesson, T. B. Coplen, T. Ding, P. J. H. Dunn, M. Gröning, N. E. Holden, H. A. J. Meijer, H. Moossen, A. Possolo, Y. Takahashi, J. Vogl, T. Walczyk, J. Wang, M. E. Wieser, S. Yoneda, X.-K. Zhu and J. Meija, *Pure Appl. Chem.*, 2022, **94**, 573–600.
45 CIAAW, *Atomic Weights of the Elements*, https://www.ciaaw.org/, accessed June 27th, 2025.
46 M. Kuonen, B. Hattendorf and D. Gunther, *J. Anal. At. Spectrom.*, 2024, **39**, 1388–1397.
47 H. Andrén, I. Rodushkin, A. Stenberg, D. Malinovsky and D. C. Baxter, *J. Anal. At. Spectrom.*, 2004, **19**, 1217–1224.
48 F. Vanhaecke, R. Dams and C. Vandecasteele, *J. Anal. At. Spectrom.*, 1993, **8**, 433–438.
49 A. Tupys, K. Tetfejer, L. Halicz, E. Bulska and J. Karasiński, *J. Anal. At. Spectrom.*, 2024, **39**, 3142–3150.
50 W. A. Russell, D. A. Papanastassiou and T. A. Tombrello, *Geochim. Cosmochim. Acta*, 1978, **42**, 1075–1090.
51 J. Fietzke and A. Eisenhauer, *Geochem., Geophys., Geosyst.*, 2006, **7**, Q08009.
52 L. Halicz, I. Segal, N. Fruchter, M. Stein and B. Lazar, *Earth Planet. Sci. Lett.*, 2008, **272**, 406–411.
53 L. Yang, C. Peter, U. Panne and R. E. Sturgeon, *J. Anal. At. Spectrom.*, 2008, **23**, 1269–1274.
54 H.-C. Liu, C.-F. You, K.-F. Huang and C.-H. Chung, *Talanta*, 2012, **88**, 338–344.
55 GeoREM, *Geological and Environmental Reference Materials*, http://georem.mpch-mainz.gwdg.de/sample_query_pref.asp, accessed June 27th, 2025.
56 S. J. Romaniello, M. P. Field, H. B. Smith, G. W. Gordon, M. H. Kim and A. D. Anbar, *J. Anal. At. Spectrom.*, 2015, **30**, 1906–1912.
57 R. A. Bertram, D. J. Wilson, T. van de Flierdt, R. M. McKay, M. O. Patterson, F. J. Jimenez-Espejo, C. Escutia, G. C. Duke, B. I. Taylor-Silva and C. R. Riesselman, *Earth Planet. Sci. Lett.*, 2018, **494**, 109–116.

58 J. M. Brazier, A. D. Schmitt, E. Pelt, D. Lemarchand, S. Gangloff, T. Tacail and V. Balter, *Geostand. Geoanal. Res.*, 2020, **44**, 331–348.
59 A. Retzmann, T. Zimmermann, D. Profrock, T. Prohaska and J. Irrgeher, *Anal. Bioanal. Chem.*, 2017, **409**, 5463–5480.
60 P. Galler, A. Limbeck, S. F. Boulyga, G. Stingeder, T. Hirata and T. Prohaska, *Anal. Chem.*, 2007, **79**, 5023–5029.
61 A. Retzmann, J. Budka, H. Sattmann, J. Irrgeher and T. Prohaska, *Egypt and the Levant*, 2019, **29**, 357–382.
62 A. Retzmann, A.-M. Kriechbaum, M. Griebl, K. Wiltschke-Schrotta, M. Teschler-Nicola, J. Irrgeher and T. Prohaska, *Archaeol. Austriaca*, 2020, 53–87.